sLHC Project Note 0032

2010-12-23

jim@stovall.net

On the Feasibility of Accelerating Deuterons in Linac4

J. Stovall, J.B. Lallement, M. Garcia Tudela, S. Ramberger, K. Crandall

Keywords: Linac4, Deuterons

Summary

The Linac4 normal-conducting linac is comprised of three sections, DTL, CCDTL and PIMS. It is designed to accelerate H-minus ions to a final energy of 160 MeV. The objective of this study is to investigate the feasibility of accelerating deuterons in this linac for injection into the PS Booster.

1. Introduction

Linac4 is comprised of 3 accelerating sections, each using a different mode of operation. The structures are: 1, the drift-tube linac (DTL), which operates in the zero or 2π mode, 2, the coupled-cavity drift-tube linac (CCDTL), which operates in a 2π-$\pi/2$ mode and 3, the pi-mode structure (PIMS), which operates in the π mode. In these three different structures the mode of operation refers to rf phase shift, in radians, between adjacent accelerating gaps. With the exception of the CCDTL, it also refers to the rf phase advance required for the synchronous particle, traveling at the design velocity β_s to advance from the center of one accelerating gap to the center of the next.

There are two conditions that must be met for successful accceleration of deuterons in LINAC4. There must be a mode of operation in which particles arrive at the center of each accelerating gap while the rf fields are in the positive direction and on average provide longitudinal stability. In addition, the magnetic focusing lattice must provide transverse stability. As a measure of both requirements we calculate the transverse and longitudinal acceptances.

2. DTL

a. Longitudinal motion

Because deuterons have half the charge-to-mass ratio of protons (H-minus ions), the integrated accelerating field seen by the deuterons in the DTL E_0 would have to be twice the nominal design value for them to remain synchronous. Because the structure is designed to operate near the sparking limit this approach is impractical. It may be practical, however, to operate the DTL in the 4π mode in which the cavity is excited at the nominal design field amplitude but the deuterons travel at half of the design velocity $\beta_s/2$ thus taking two rf periods to traverse each cell. Because the charge and momentum of deuterons travelling at half velocity is the same as that of protons (H-minus) we would expect the properties of the transverse focusing lattice to be similar for both ions.

To investigate how these off-energy particles fare in all three sections of the linac, we have written a code that integrates the ion's longitudinal motion through axial field maps E(0,z) for each structure. While there are standard codes that integrate particle motion through the

fields in accelerators we found it simpler for this feasibility study to write a general purpose code that addressed only the longitudinal motion of particles on axis. By modifying the ion's rf phase and velocity at injection of each section we can observe if and how well they are accelerated and calculate the transverse and longitudinal acceptance of each section.

The DTL is designed to have a "flat" average axial electric field amplitude E_0 throughout. We define a cell of length L as beginning and ending in the middle of a drift tube.

$$\mathbf{E_0} = \frac{\mathbf{1}}{\mathbf{L}} \int_{-\frac{\mathbf{L}}{\mathbf{2}}}^{\frac{\mathbf{L}}{\mathbf{2}}} \mathbf{E(0,z)dz}$$

$$\text{where } L = \beta s\, \lambda \left(\frac{2\pi - \Delta\phi s}{2\pi}\right)$$

Figure 1 shows the axial rf field distibution E(0,z) computed by the cavity code Superfish in the first tank of the DTL. Figure 2 shows that E_0, numerically integrated from the fields in figure 1 for each cell, is in fact flat in tank 1. The synchronous phase ϕ_s is ramped linearly in the tank to provide strong longitudinal focusing in the initial cells and efficient acceleration in the later cells. As we see in figure 3, ϕ_s deviates from the linear ramp in the last 3 cells. This design feature provides additional longitudinal focusing to compensate for the two missing gaps between tanks 1 and 2. Figure 4 shows the actual fields seen by the protons as they traverse the tank. Figure 5 shows the energy profile for the protons in tank 1 by integrating the particle motion through these fields. Figure 6 shows the longitudinal acceptance for protons in tank 1.

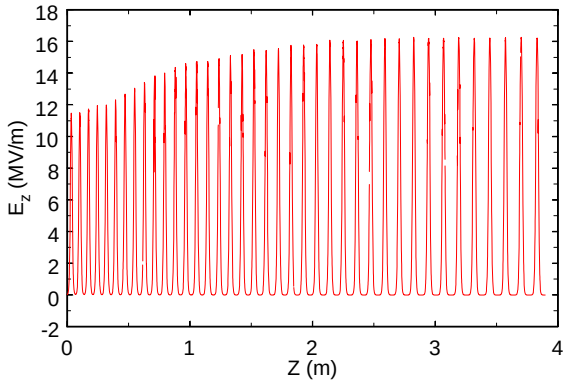

Figure 1, Axial field distribution in DTL tank 1

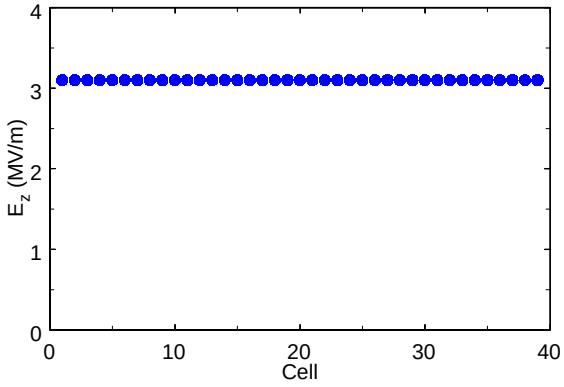

Figure 2, E_0 in DTL tank 1

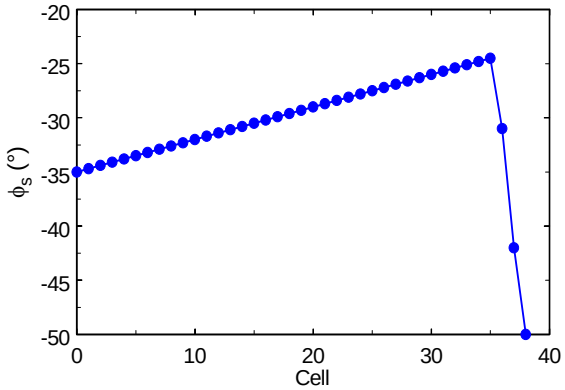

Figure 3, ϕ_s in DTL tank 1 in DTL tank 1

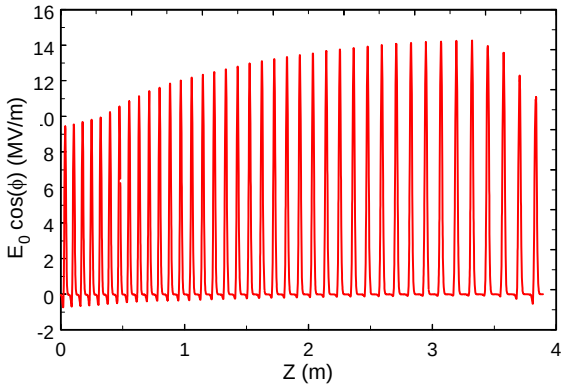

Figure 4, Axial field seen by the proton reference particle in DTL tank 1

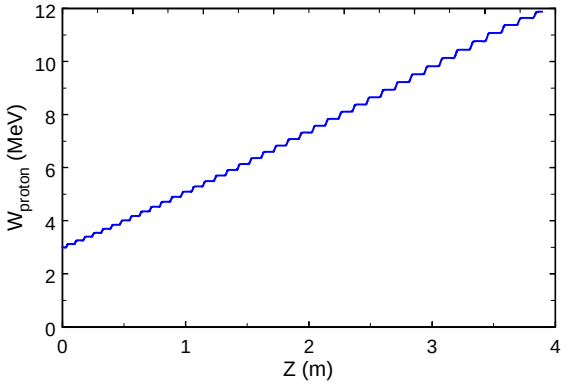

Figure 5, Energy profile of the proton reference particle in DTL tank 1

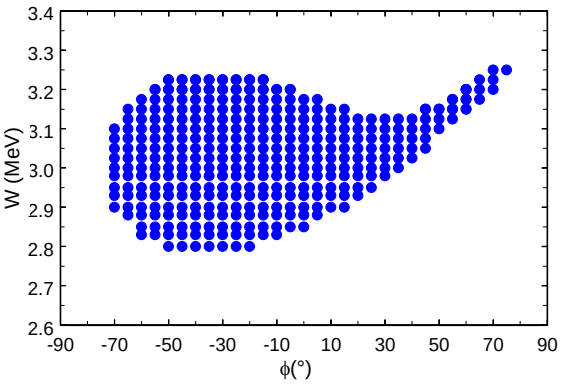

Figure 6, DTL Tank 1 longitudinal acceptance for protons

Deuterons injected at half the design velocity $\beta_s/2$ into tank 1 remain nominally synchronous with the rf but take two periods of the rf to travel from the center of one cell to the center of the next. Figure 7 shows the rf fields seen by the deuterons injected at half velocity and at a phase that minimizes the longitudinal phase oscillation. Because the deuterons are moving so slowly they see decelerating fields as they both enter and exit each gap. We deem the longitudinal motion to be stable because, while the phase oscillates, the ions continue to gain approximately the correct amount of energy as we can see in figure 8.

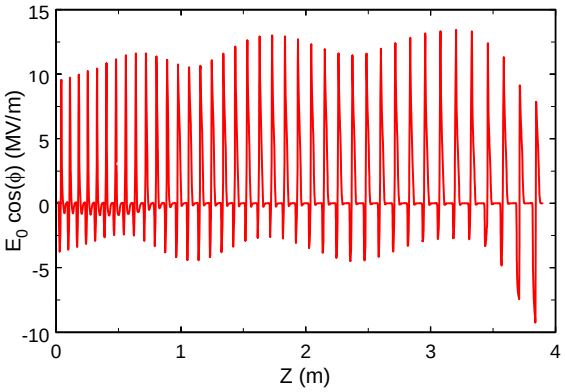

Figure 7, Axial field seen by a deuteron reference particle in DTL tank 1

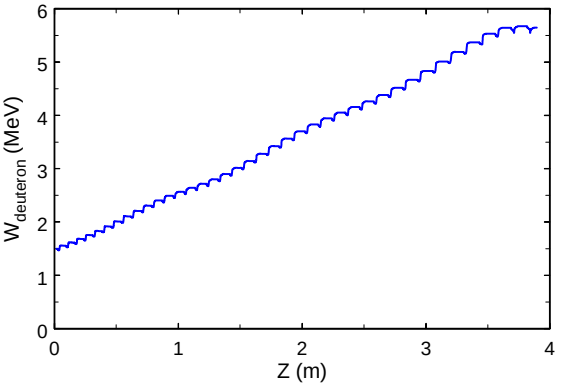

Figure 8, Energy profile of a deuteron reference particle in DTL tank 1

Until the last 3 cells, the deuterons remain nominally synchronous with the structure at half velocity. In the final cells, however, they fall out of synchronism due to the phase programming imposed to compensate for the missing gaps between tanks 1 and 2 for protons. We see this effect in the energy-gain plot in figure 8 where deuterons are actually decelerated in the final cell.

Figure 9 shows the longitudinal acceptance for deuterons in tank 1. Like the acceptance for protons, it is large and symmetrical, having the classical shape**.** Figure 10 shows the longitudinal acceptance for deuterons in tank 2 which is also large and symmetrical. As figure 8 shows, the final energy for deuterons accelerated in tank 1 is about 350 keV low because of the phase programming in the final three cells. We can see this effect again in figure 10 where we have superimposed the output phase-space coordinates of the "accepted" particles from tank 1 onto the acceptance of tank 2. It is clear that most of the deuterons accelerated in tank 1 will not be captured in tank 2.

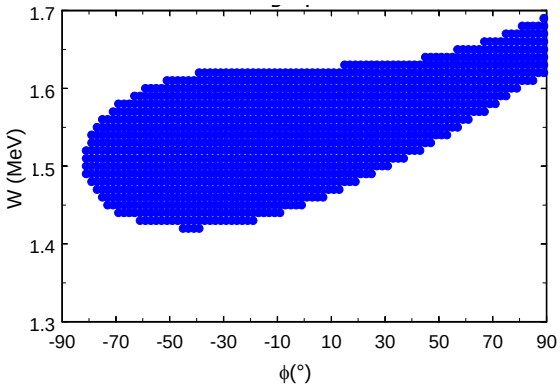

Figure 9, DTL Tank 1 longitudinal acceptance for deuterons at $\beta_s/2$

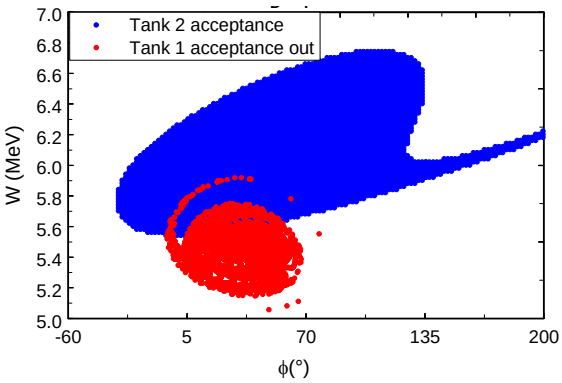

Figure 10, DTL Tank 2 longitudinal acceptance for deuterons at $\beta_s/2$

b. Transverse motion

The code used to evaluate the longitudinal motion above uses only the axial electric field, E(0,z). To study the transverse motion we have used PathManager, a "lumped-element" code in which the energy gained cell-by-cell ΔW is calculated using the well known "Panofsky equation."

$$\Delta W = qE_0TL\cos\phi_S$$

E_0 is a design constant (figure 2) and is independent of particle velocity. T, the transit-time factor, is the ratio of the energy gained by an ion of charge q traversing a cell in the time-varying rf field to the energy gained in a dc field having the voltage $V_0 \cos \phi_S$. L is the cell length $\beta_S\lambda$ and ϕ_s is the design synchronous phase. To simplify the calculation of T we assume that the electrical and mechanical centers of the cells coincide. (1)

$$T = \frac{\int_{-L/2}^{L/2} E(0,z)\cos\omega t(z)dz}{\int_{-L/2}^{L/2} |\,E(0,z)\,|\,dz}$$

where $\omega_{deuterons}=2\omega_{protons}$

Figure 11 shows the transit-time factors for protons and for deuterons in tank 1 computed by integrating the time-varying axial fields E(0,z) (figure 1) through each cell. We also plot the ratio of T for deuterons to T for protons T_d/T_p and see that it exceeds ½ throughout most of the tank.

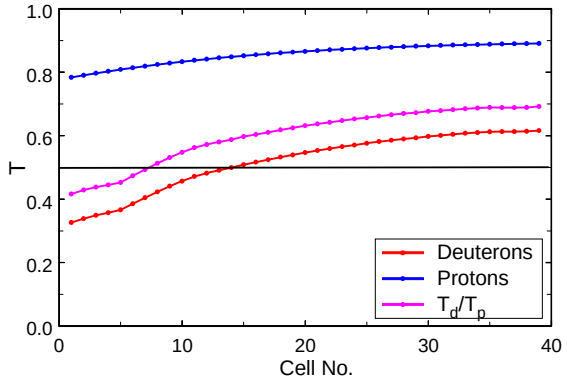

Figure 11, T for protons and deuterons in DTL tank 1

Although the longitudinal acceptance for deuterons is large and the acceleration appears to be stable, the transverse dynamics are much less attractive. Figure 12 shows the phase of both proton and deuteron reference particles, calculated by PathManager, as they cross the center of each gap. We see that the reference proton follows the design phase ϕ_s which is linearly ramped from -35° to -24.5° (figure 3). The reference deuteron however follows the reference phase for only about 7-8 cells, to the point at which T_p/T_d becomes greater than ½, then seeks a new stable phase at about -50° about which it oscillates.

In this example the reference deuteron was injected at half velocity and arrives at the first gap at -35°. We have investigated changing the injection energy, the initial phase and the rf field amplitude in an attempt to minimize the phase oscillation but in all cases we find that a reference deuteron eventually seeks a large stable phase at about -50° about which it oscillates.

In the design of the DTL we have tailored the strength of the transverse focusing lattice to balance both space charge and the longitudinal rf defocusing forces while avoiding all known resonances. We define the radial impulse delivered to particle from the RF fields in the gap. (2)

$$\Delta(\beta\gamma r') = -q\frac{\gamma_s(1-\beta\beta_s)}{mc^2\beta}E_0TI_1(Kr)\sin\phi$$

Assuming only the particle trajectories that are close to the axis we can simplify this equation.

$$\Delta(r'/r) = \frac{-q\pi E_0TL}{mc^2\lambda}\frac{(1-\beta\beta_s)}{\gamma_s\beta^2\beta_s}\sin\phi$$

Figure 13 shows the the defocusing force $\Delta(r'/r)$ for both protons and deuterons when operating tank 1 at the design accelerating field. Here we can see that both E_0T and ϕ are too large essentially doubling the radial impulse seen by deuterons.

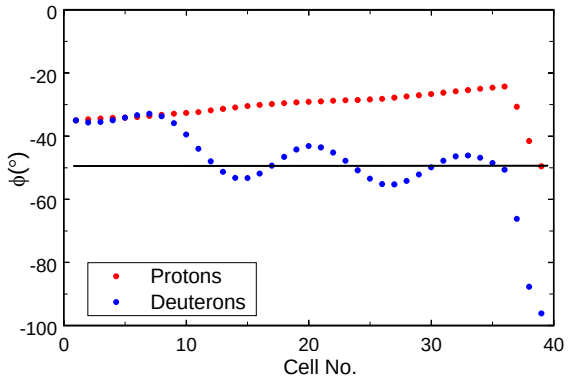

Figure 12, Phase of the proton and deuteron reference particles in DTL tank 1

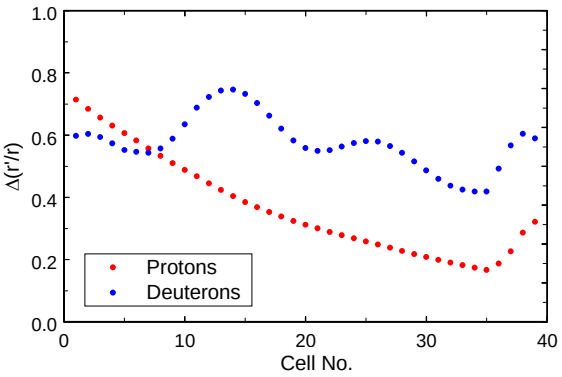

Figure 13, RF defocusing force seen by protons and deuterons in DTL tank 1

The transverse acceptance for protons in tank 1 is large and symmetrical as shown in figure 14. As a consequence of the large rf defocusing forces seen by deuterons, the restoring force provided by the magnetic focusing lattice after about cell 8 is wholely inadequate as shown by the transverse acceptance plotted in figure 15.

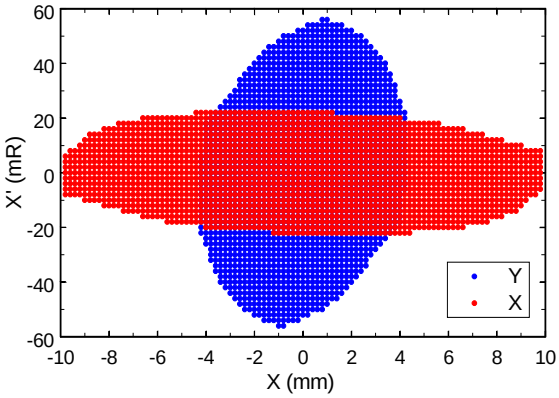

Figure 14, Transverse acceptance for protons in DTL tank 1

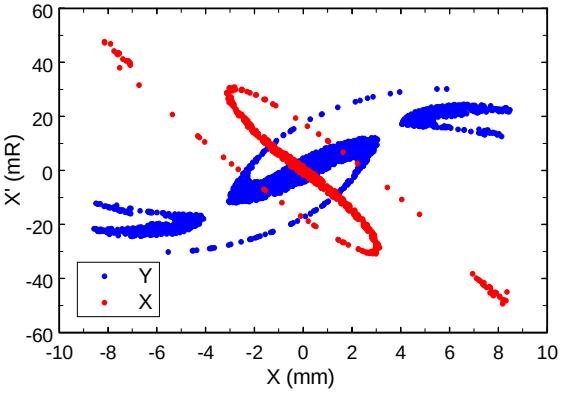

Figure 15, Transverse acceptance for deuterons in DTL tank 1

Figure 16 shows the expected beam profiles for a deuteron beam traveling at $\beta_S/2$ in tank 1 as simulated by a version of Trace3D that tracks the phase of the beam centroid through each element. As expected, a matched beam remains stable transversely in the first few cells but as we have seen in figure 13 it then becomes strongly defocused by the rf causing it to dramatically blow up transversely. As the effective ϕ_S becomes more negative the beam is strongly focused longitudinally, reducing its phase profile.

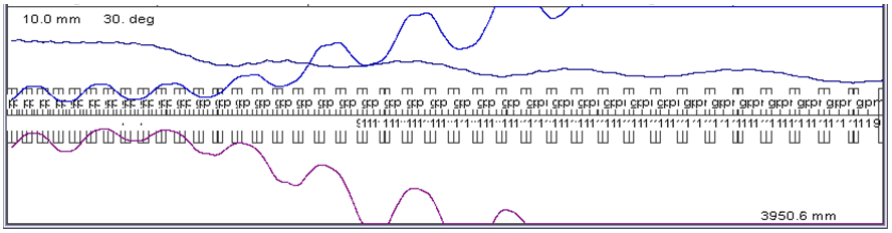

Figure 16, Longitudinal and transverse beam profiles for deuterons in DTL tank 1

Ideally the integrated field seen by deuterons E_0T_d would equal half of that seen by protons or $E_0T_p/2$ to maintain syncronism at half velocity. We could achieve this condition in practice by retuning the field distribution in tank 1 to introduce a reverse ramp as shown in figure 17 (compare with figure 1). In this case PathManager shows that the phase of the reference deuteron closely follows the design phase law as we see in figure 18.

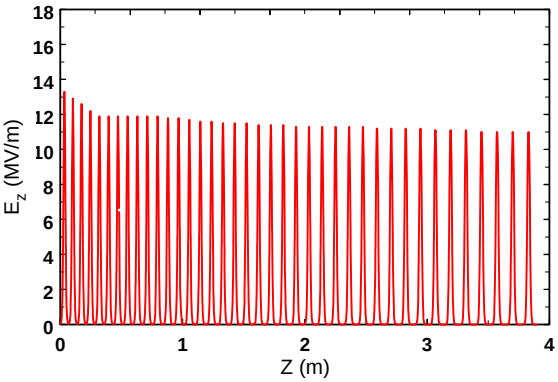

Figure 17, Axial field distribution in tank 1 retuned to accelerate deuterons

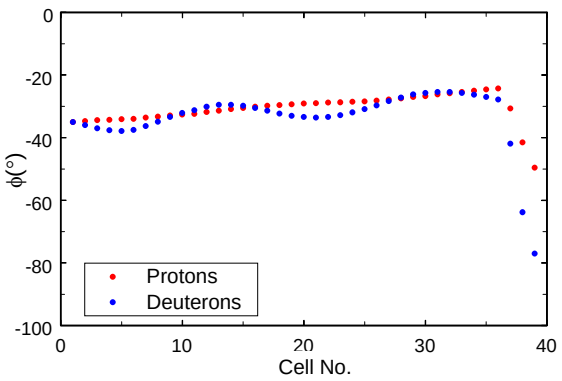

Figure 18, Phase of the reference proton and deuteron in DTL tank1 retuned

By tuning the fields to the correct E_0T_d profile we can not only correct the phase motion of the deuterons but we also see in figure 19 that the resulting rf defocusing forces closely follow those of the design values that are balanced by the magnetic focusing lattice as we see

from the large transverse acceptance in figure 20. Figure 21 shows that the expected profiles for a deuteron beam are well behaved under these conditions.

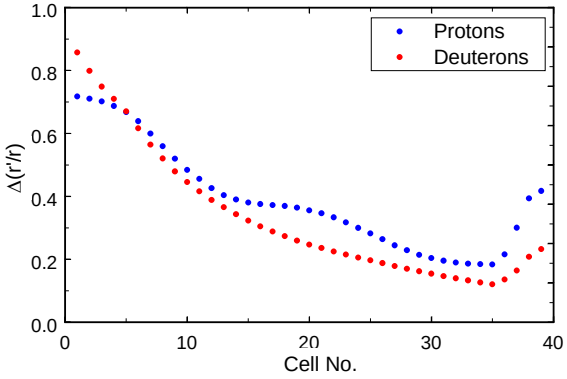

Figure 19, RF defocusing forces seen by protons and deuterons in DTL tank1 retuned

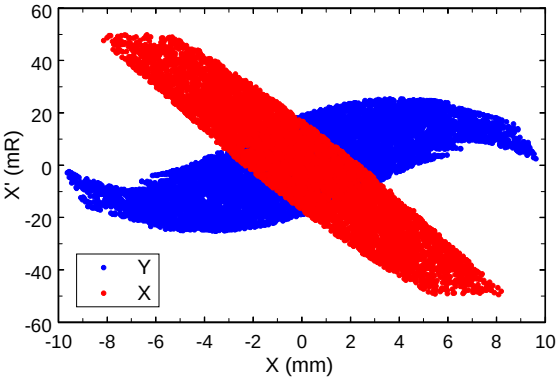

Figure 20, Transverse acceptance for deuterons in DTL tank 1

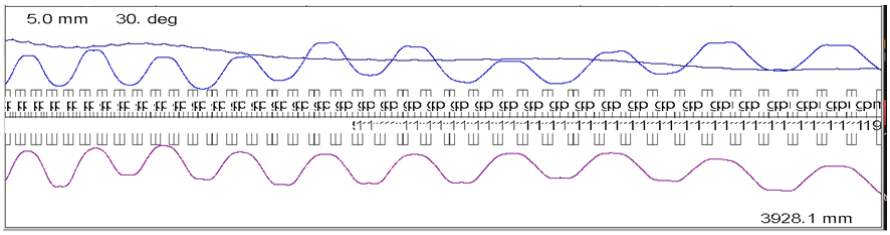

Figure 21, Longitudinal and transverse beam profiles for deuterons in DTL tank 1 retuned

3. CCDTL

Figure 22 shows a cross section view of one module of the CCDTL structure. It is comprised of three constant-β DTL cavities resonantly coupled together in the π/2-mode. Protons entering the structure at the synchronous velocity β_s advance from gap-to-gap in one period of the rf. They require 3/2 rf periods to travel between accelerating cavities in which the fields are reversed. Figure 23 shows the axial electric field distribution in the first module of the CCDTL. Figure 24 shows the fields seen by protons traveling at β_s while figure 25 shows the energy-gain profile of the protons.

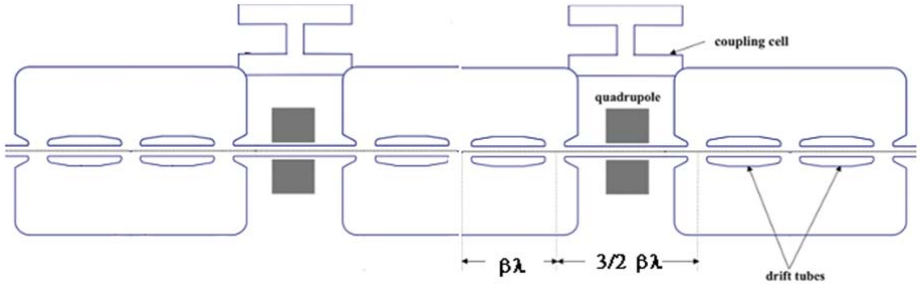

Figure 22, CCDTL

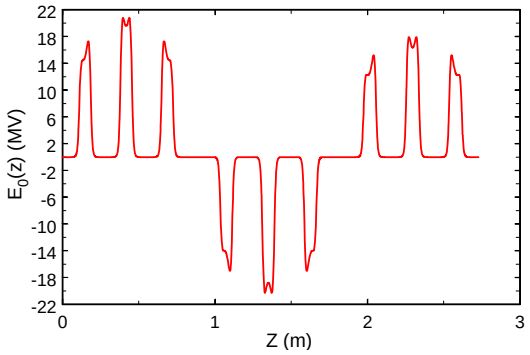

Figure 23, Axial field distribution in CCDTL module 1

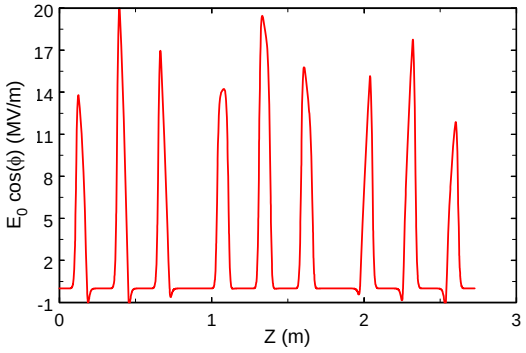

Figure 24, Fields seen by protons traveling at β_s in CCDTL module 1

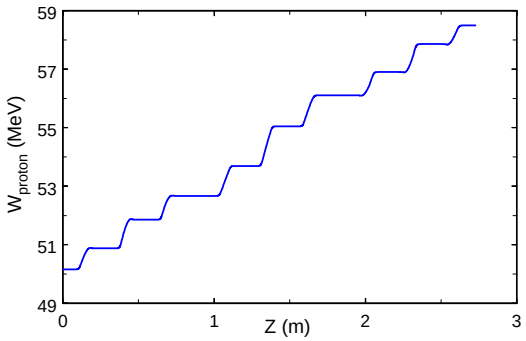

Figure 25, Energy gained by protons traveling at β_s in CCDTL module 1

Deuterons injected into this structure at half the design velocity $\beta_s/2$ remain synchronous through the first tank. However, they would arrive at the second tank when the fields are in the reverse direction. The next option is to inject deuterons at one third the design velicity $\beta_s/3$. Figure 26 shows the fields seen by deuterons traveling at $\beta_s/3$ through the first CCDTL module. At such a low velocity this is a very inefficient mode of operation.

The average gap-to-$\beta_G\lambda$ ratio in the first tank is 0.275. Because deuterons spend 3 rf periods in each cell they would spend an average of 297° in each accelerating gap, not including the effect of the fields that extend into the bore of the drift tube. The transit-time factor for this structure is $\leq$0.1 when operating in the 6π mode for deuterons compared to ~0.84 when operated in the 2π mode for protons. As a result the rate of acceleration is very poor and the deuterons cannot maintain synchronism with the structure. Figure 27 shows the energy-gain profile for deuterons in module 1 of the CCDTL traveling at $\beta_s/3$ which is <10% of the energy gained by protons.

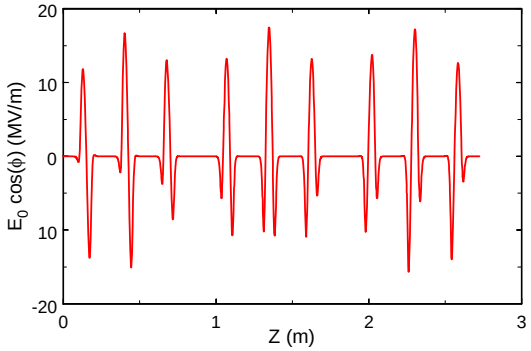

Figure 26, Field seen by deuterons traveling at βs/3 in CCDTL tank 1

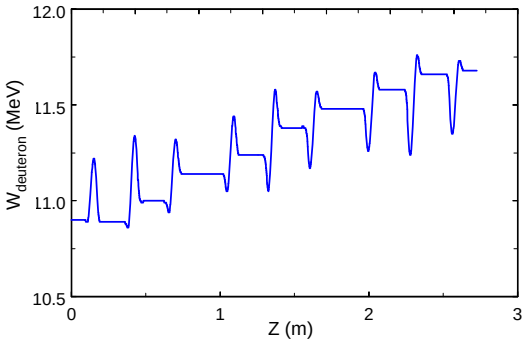

Figure 27, Energy gained by deuterons traveling at $\beta_s/3$ in CCDTL tank 1

4 PIMS

Figure 28 shows a cross section view of one module of the PIMS structure. It is comprised of seven constant-β cavities resonantly coupled together in the π-mode. Protons entering the structure at the synchronous velocity β_s will advance from gap-to-gap in one half of an rf period. Figure 29 shows the axial electric field distribution in the first module of the PIMS. Figure 30 shows the fields seen by protons traveling at β_s while figure 31 shows the energy-gain profile of the protons.

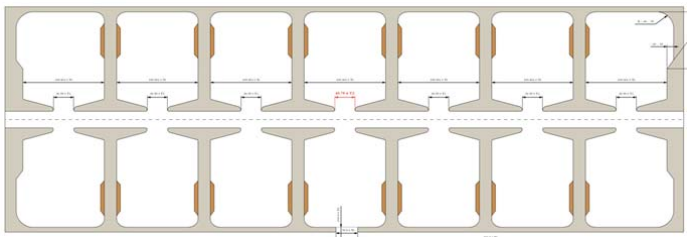

Figure 28, PIMS

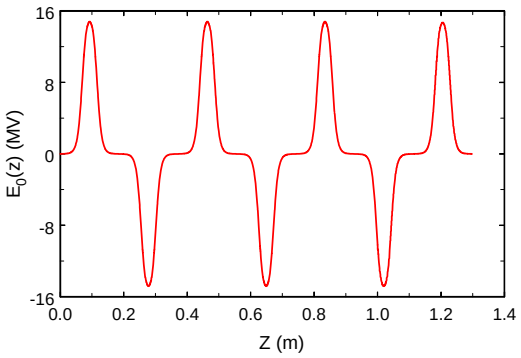

Figure 29, Axial field distribution in PIMS module 1

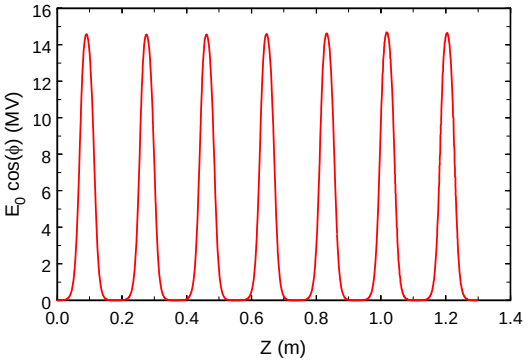

Figure 30, Fields seen by protons traveling at β_s in PIMS module 1

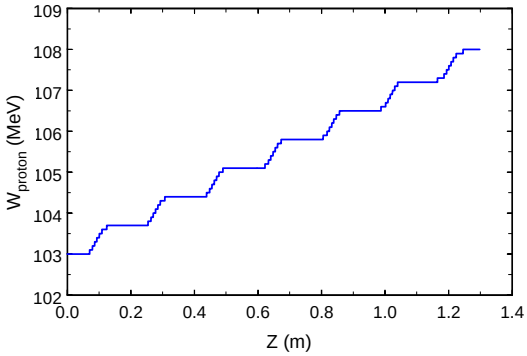

Figure 31, Energy gained by protons traveling at β_s in PIMS module 1

Deuterons injected into this structure at half the design velocity $\beta_s/2$ arrive at the second gap when the fields are in the reverse direction. The next option is to inject deuterons at one third the design velicity $\beta_s/3$. Figure 32 shows the fields seen by deuterons traveling at $\beta_s/3$ through the first PIMS module. With a transit-time factor of 0.64 when operated in the 3π mode compared to 0.95 when operated in the π mode, the PIMS is a relatively good accelerator for deuterons. Figure 32 shows that there is an apparent phase slippage through the 7-cell cavity. We believe that this is just part of an otherwise stable phase oscillation. Figure 33 shows the energy-gain profile for deuterons in module 1 of the PIMS traveling at $\beta_s/3$. Although deuterons only gain a third of the velocity gained by protons, they gain more than half of the energy gained by protons because of relativistic effects.

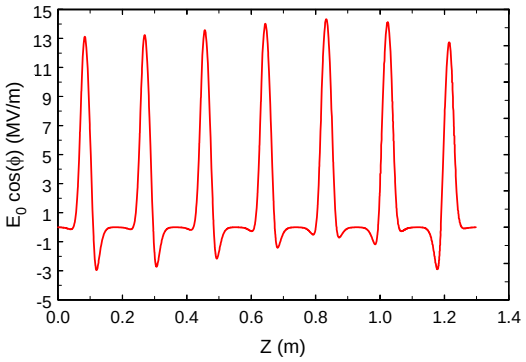

Figure 32, Field seen by deuterons traveling at βs/3 in PIMS tank 1

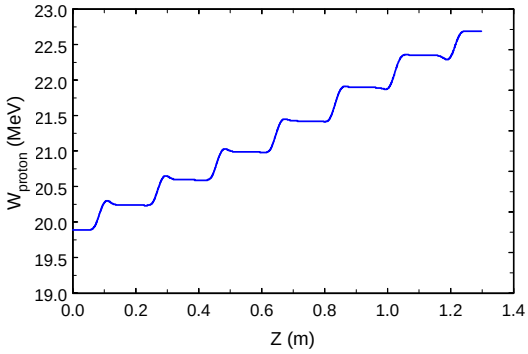

Figure 33, Energy gained by deuterons traveling at $\beta_s/3$ in PIMS tank 1

5 Conclusions

We have found that, while the DTL has a large longitudinal acceptance for deuterons injected at $\beta_S/2$, the transverse rf defocusing is too strong when operating at the design field level resulting in excessive transverse beam loss. Just decreasing the field amplitude does not help. To efficiently accelerate deuterons would require retuning the field distribution in tank 1 to introduce a reverse field ramp. In this study we have not investigated the feasibility of introducing such a field distribution. The CCDTL is a very poor accelerator for deuterons even if we could inject a beam at $\beta_S/3$. Because it is very unlikely that we could provide an appropriate beam for injection into the CCDTL we have not investigated its transverse properties. The PIMS might be a reasonable accelerator for deuterons and benefits from having electromagnetic lenses that we could use to tailor the transverse focal properties. However, it is unlikely that we could provide a beam at the required injection energy so we have not

investigated its transverse properties. We conclude that Linac4 is not a good candidate for accelerating deuterons.

6 Acknowledgement

The authors would like to acknowledge the helpful discussions with their colleague Jean-Michel Lagniel.

---

1. **Wangler, T.** *Principles of RF Linear Accelerators.* s.l. : John Wiley & Sons, Inc., 1998. eqn(4.5).

2. **Ibid.** eqn.(7.6).